Materials Chemistry and Physics 125 (2011) 196–201

Contents lists available at ScienceDirect

Materials Chemistry and Physics

journal homepage: www.elsevier.com/locate/matchemphys

Flame retardancy and thermal properties of epoxy acrylate resin/alpha-zirconium phosphate nanocomposites used for UV-curing flame retardant films

Weiyi Xing[a,b], Ganxin Jie[c], Lei Song[a], Xin Wang[a], Xiaoqi Lv[a], Yuan Hu[a,b,*]

[a] State Key Laboratory of Fire Science, University of Science and Technology of China, 96 Jinzai Road, Hefei, Anhui 230026, PR China
[b] Suzhou Institute for Advanced Study, University of Science and Technology of China, 166 Ren'ai Road, Suzhou, Jiangsu 215123, PR China
[c] State Key Laboratory of Environmental Adaptability for Industrial Products, China National Electric Apparatus Research Institute, Guangzhou 510300, PR China

ARTICLE INFO

Article history:
Received 8 June 2010
Received in revised form 19 August 2010
Accepted 1 September 2010

Keywords:
Thermal degradation
Flame retardancy
UV-curing
OZrP
Nanocomposites

ABSTRACT

This paper reported the UV-curing flame retardant film, which consisted of epoxy acrylate resin (EA) used as an oligomer, tri(acryloyloxyethyl) phosphate (TAEP) and triglycidyl isocyanurate acrylate (TGICA) used as flame retardant (FR). The flame retardancy and thermal properties of films were reinforced by using alpha-zirconium phosphate (α-Zr $(HPO_4)_2H_2O$, α-ZrP). The morphology of nanocomposite film was characterized by X-ray diffraction (XRD) and transmission electron microscopy (TEM). The results showed that the organophilic α-ZrP (OZrP) layers were dispersed well in epoxy acrylate resin. Microscale Combustion Calorimeter (MCC), thermogravimetric analysis (TGA) and thermogravimetric analysis/infrared spectrometry (TGA-IR) were used to characterize the flame retardant property and thermal stability. It was found that the incorporation of TAEP and TGICA can reduce the flammability of EA. Moreover, further reductions were observed due to the addition of OZrP. The char residue for systems with or without OZrP was also explored by scanning electron microscopy (SEM).

1. Introduction

The applications of UV-curable film have gained wide interests, due to their advantages such as lower energy consumption, less environmental pollution, lower process costs, high chemical stability and very rapid curing even at ambient temperature [1–3]. Epoxy acrylate resins (EA) are extensively used as oligomers in UV-curable systems and form three-dimensional polymeric networks by curing [4,5]. Moreover, they are mostly used for high-performance applications because of their unique performance-to-cost ratio and because they can produce hard and chemically resistant films compared with other oligomers. However, epoxy acrylate resins are flammable, which could restrict some applications. Therefore, there is an urgent need to explore flame retardant UV-curable coating to reduce the fire hazards.

Traditionally, flame retardant films could be obtained by physically blending flame retardants. However, the high concentration of flame retardants in the coatings results in difficulty to cure and deteriorated properties [6]. When used in coatings, phase separation often takes place, which will cause cracks on the surface of films [7]. Another efficient approach to reduce the flammability of the cured films is through chemically bonding flame retardant segments to the polymer backbone [8], i.e., using UV-curable reactive flame retardants. The reactive-type flame retardants are interesting due to their many advantages in comparison with additive-type ones. On the one hand, they can promote the condensed phase mechanism, especially flame retardants containing phosphorus [9]. On the other hand, reactive-type flame retardants can work longer as they will not exude from polymer materials during use and aging [10]. Generally speaking, all of the UV-curable reactive flame retardants contain one or more flame retardant elements, such as P, N, Si, and B elements. Some phosphorus-containing compounds have been used to increase the limiting oxygen index (LOI) and char residues [11,12]. Shi and her coworkers reported that the flame retardant films containing nitrogen have high thermal stability compared with pure epoxy acrylate resins [13].

Recently, organic–inorganic nanocomposites have drawn increased attention because of their distinct characteristics, in particular superior mechanical and barrier properties, as well as improved thermal stability, flame retardancy and optical properties. Moreover, there has been considerable interest in the preparation of nanocomposites based on layered materials as guests and polymers as hosts [14]. These layered materials include layered silicates [15], manganese oxides [16], titanates [17] and layered phosphates [18]. In recent papers, UV-curing technology has been used to produce rapidly the organic–inorganic

* Corresponding author at: State Key Laboratory of Fire Science, University of Science and Technology of China, 96 Jinzai Road, Hefei, Anhui 230026, PR China. Fax: +86 551 3601664.
E-mail address: yuanhu@ustc.edu.cn (Y. Hu).

0254-0584/$ – see front matter © 2010 Published by Elsevier B.V.
doi:10.1016/j.matchemphys.2010.09.006

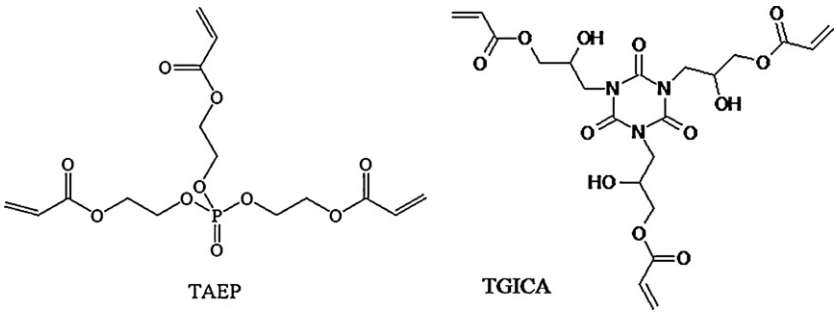

Fig. 1. The molecular structures of TAEP and TGICA.

hybrid materials at ambient temperature. Zahouily et al. first demonstrated UV-curable polymer–clay nanocomposites could be prepared [19]. Bauer et al. examined the performance of nanoparticle reinforced acrylate resins. The results revealed that UV-cured nano/microhybrid composites had a significant abrasion resistance [20].

Among the nanofillers, clay compounds are most widely used for preparing polymer nanocomposites, because these compounds are easily available and well characterized. Alpha-zirconium phosphate (α-Zr $(HPO_4)_2{\cdot}H_2O$, α-ZrP), is a crystalline, layered material with many notable features, such as ion-exchange properties, thermal and chemical stability [21], catalytic activity and intercalation properties in polymers. However, only a few investigations have been conducted on polymer/α-ZrP nanocomposites [22], including the preparation and characterization of PET/α-ZrP nanocomposites [23] and epoxy/α-ZrP nanocomposites [24]. To our knowledge, the study of flame retardant epoxy acrylate resin/α-ZrP nanocomposites has not been reported.

In this study, a phosphorous-containing monomer (TAEP) and a nitrogen-containing monomer (TGICA) were incorporated into the epoxy acrylate structures. And then α-ZrP was introduced to EA resin to prepare the UV-curable polymer/α-ZrP nanocomposite. The enhanced thermal and flame retardant properties of the nanocomposite were investigated in detail.

2. Experimental

2.1. Materials

EA, which is a bisphenol A epoxy acrylate with the unsaturation concentration of 3.73 mmol g^{-1} and a molar mass of 536 g mol^{-1}, was supplied by Tianjin Tianjiao Co. OZrP powder was prepared by hydrothermal synthesis under the optimum condition according to our previous work [25]. TAEP was synthesized using phosphorus oxychloride and 2-hydroxylethyl acrylate [26]. TGICA was synthesized using acrylic acid and triglycidyl isocyanurate [27]. The molecular structures of TAEP and TGICA are shown in Fig. 1. Tetrahydrofuran (THF) was purchased from Shanghai Chemical Reagents Company in China. 2-Hydroxy-2-methyl-1-phenyl-1-propanone (Darocur 1173), kindly supplied by Ciba Specialty Chemicals, was used as a photoinitiator.

2.2. Preparation of the samples

To prepare EA/FR/OZrP nanocomposite, a certain amount of OZrP powder was dispersed in solution containing flame retardant (listed in Table 1), then carried out ultrasonic treatment for 1 h, and thereafter EA solution was added into above solution, and then carried out ultrasonic treatment for 3 h again, stirred for 24 h at ambient temperature, finally.

Table 1
The formulations and the MCC data of the cured films.

Sample	EA (%)	FR (%)	OZrP (%)	PHRR (W g^{-1})	HRC (J $(g\,K)^{-1}$)
EA0	100	0	0	332 ± 8	340 ± 8
EA1	60	40	0	193 ± 13	195 ± 11
EA2	60	39	1	142 ± 6	143 ± 4
EA3	60	37	3	167 ± 15	163 ± 7
EA4	60	35	5	177 ± 7	179 ± 9

FR: TAEP/TGICA = 1/1, by weight.

2.3. UV irradiation process of EA/FR/OZrP nanocomposite

The samples were UV-cured with UV irradiation equipment (80 W cm^{-2}, made by Lantian Co.) in the presence of 4 wt% Darocur 1173. The UV irradiation was carried out in air atmosphere.

3. Measurements

3.1. X-ray diffraction (XRD) analysis

X-ray diffraction analysis was carried out on sample at room temperature by a Japan Rigaku D/max-rA X diffraction meter (30 kV, 10 mA) with Cu (λ = 1.54178 Å) irradiation at the rate of 2° min^{-1} in the range of 1–10°. The interlayer distance of OZrP and nanocomposites was calculated using Bragg's law.

3.2. Transmission electron microscopy (TEM)

Transmission electron microscopy (TEM) images were obtained on a Jeol JEM-100SX transmission electron microscope with an acceleration voltage of 100 kV. The TEM specimens were cut at room temperature using an ultramicrotome (Ultracut-1, UK) with a diamond knife from nanocomposite films. Thin specimens, 50–80 nm, were collected in a trough filled with water and placed on 200 mesh copper grids.

3.3. Microscale Combustion Calorimeter (MCC)

GOVMARK MCC-2 Microscale Combustion Calorimeter was used to investigate the combustion behavior of the UV-cured film. In this system, about 5 mg samples of UV-cured film was heated to 700 °C at a heating rate of 1 °C s^{-1} in a stream of nitrogen flowing at 80 cm^3 min^{-1}. The volatile, anaerobic thermal degradation products in the nitrogen gas stream are mixed with a 20 cm^3 min^{-1} stream of pure oxygen prior to entering a 900 °C combustion furnace. Measured parameters during the test are the heat release rate dQ/dt (W) and sample temperature as a function of time at constant heating rate [28,29]. The specific heat release rate HRR (W g^{-1}) is obtained by dividing dQ/dt at each interval by the initial sample mass. A derived quantity, the heat release capacity HRC (J $(g\,K)^{-1}$) is obtained by dividing the maximum value of the specific heat release rate by the heating rate in the test. The heat release capacity is a molecular level flammability parameter that is a good predictor of flame resistance and fire behavior when only research quantities are available for testing [30]. Peak heat release rate (PHRR) is the peak of HRR. PHRR has been found to be one of the most important parameters to evaluate fire safety. For each formulation, the test was repeated three times, for this reason standard deviation was reported for each measurement.

3.4. Scanning electron microscopy (SEM)

The char formed after Microscale Combustion Calorimeter testing was first sputter-coated with a conductive layer, and then its morphologic structures were observed by scanning electron microscopy Hitachi X650.

3.5. Thermogravimetric analysis (TGA)

The thermogravimetric analysis (TGA) was carried out on the TGA Q5000 IR thermogravimetric analyzer (TA instruments) using a heating rate of 20 °C min^{-1} in nitrogen atmosphere. In addition, $T_{-10\%}$ is the decomposition temperature at 10% weight loss. The samples were run in triplicate; the temperature reproducibility of the instrument is ±1 °C while the mass reproducibility is ±0.2%.

3.6. Thermogravimetric analysis-infrared spectrometry (TGA-IR)

Thermogravimetric analysis/infrared spectrometry (TGA-IR) of the cured sample was performed using the TGA Q5000 IR thermogravimetric analyzer that was interfaced to the Nicolet 6700 FTIR spectrophotometer. About 5.0 mg of the UV-cured sample was put in an alumina crucible and heated from 30 to 600 °C. The heating rate was set as 20 °C min^{-1} (nitrogen atmosphere, at flow rate of 45 ml min^{-1}).

4. Results and discussion

4.1. Microstructure of EA/FR/OZrP nanocomposites

XRD and TEM were used to study the morphology and dispersion state of OZrP in films. Fig. 2 shows the XRD patterns of OZrP, EA2, EA3 and EA4. About OZrP curve, the main peak at lower angles ($2\theta = 2.9$) corresponds to the interlayer distance between planes of 3.04 nm. However, in a polymer layered nanocomposites, the *d*-spacing value increases when the polymer is intercalated within the lamellar planes of the filler: in this way, in the XRD pattern a shift of the main peak to lower angles is registered, as in the case of EA4. Indeed, in this case, the peak of the filler shifts from $2\theta = 2.9$ to $2\theta = 2.04$ with a corresponding increase of the interlayer distance from 3.04 to 4.33 nm [22]. But for EA2 curve, there is no peak within the range of 2–10°. The results are derived from that the OZrP nanosheets could be sufficiently exfoliated or randomly dispersed in the epoxy acrylate resins.

Moreover, TEM results reveal the presence of singular lamellae homogenously distributed and dispersed at nanometric scale within the EA matrix, as shown in Fig. 3. This means a partial exfoliation of the filler in some regions of the compound close to zones where there is still intercalation.

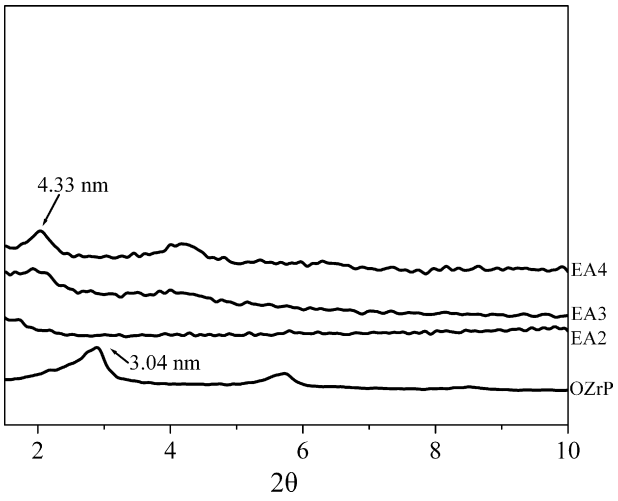

Fig. 2. X-ray diffraction analyses of OZrP and EAs.

4.2. The flame retardancy of the UV-cured films

The Microscale Combustion Calorimeter (MCC) was one of the most effective bench scale methods for investigating the combustion properties of polymer materials [31,32]. Fig. 4(a) and Table 1 outline the results obtained from MCC instrument. It can be seen that the peak heat release rate of the EA1 or nanocomposites is reduced significantly compared with that of pure EA. The incorporation of flame retardant notably reduced the flammability of epoxy acrylate resin, as that the HRC of EA1 is lower than that of pure EA. For the EA/OZrP samples, a further reduction about HRC and PHRR is observed in comparison with pure EA. It can be concluded by the following reasons. Firstly, TAEP and TGICA are able to increase the conversion of organic matter to efficient char, and thus decrease the amount of flammable volatile gases reaching the flame zone, accordingly protecting the polymeric material from further degradation. Secondly, OZrP could further retard the degradation of polymer due to the dispersion of OZrP exfoliated or intercalated nanometer sheets, promote films forming more effective protective char layer and reduce the release rate of inflammable gas. Thirdly, the water between the lamellar structures of OZrP may absorb the heat release from films, and produce the incombustible gas, which could dilute the flammable volatiles.

According to the literature, it is representative of a non-interacting behavior among the components if the calculated curve is a linear combination of the MCC curves of the individual components of the system [33]. The experimental EA2 curve and calculated EA2 are shown in Fig. 4(b). It can be seen that the peak heat release rate for experimental EA2 is much lower than the cal-

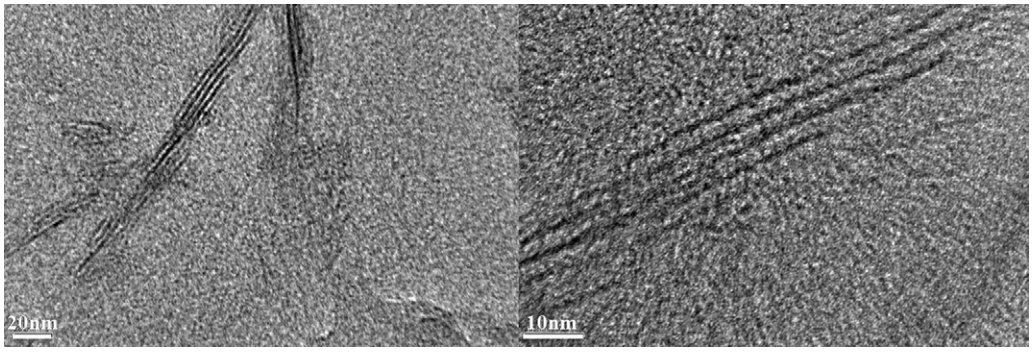

Fig. 3. The TEM image of EA3.

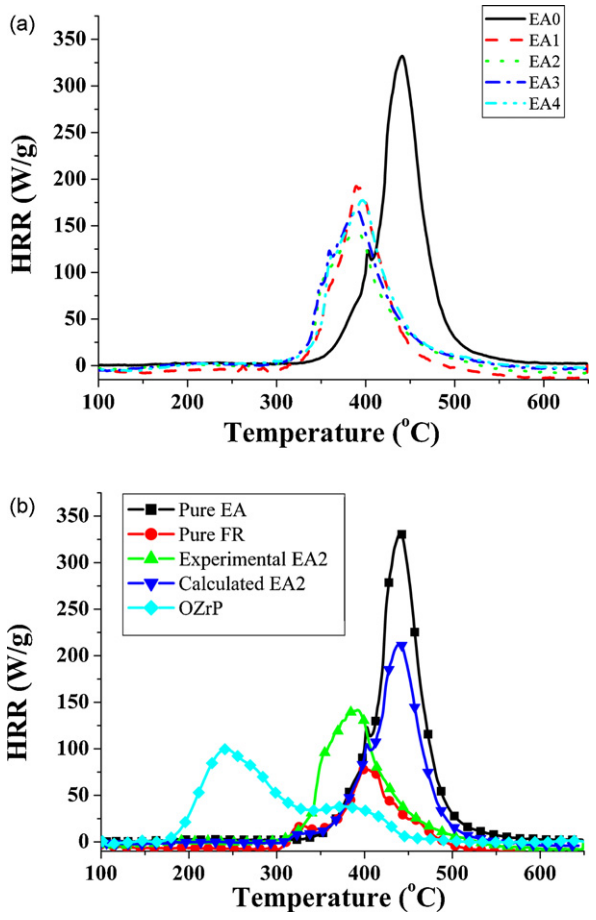

Fig. 4. MCC curves of the cured films.

culated one, which indicates the occurrence of an reaction among OZrP, FR and EA during heating, not only simply physical blending.

4.3. Characterization of the char layer

The high quality char acts as an insulating barrier during degradation. The protective barrier can limit the volatiles diffusion to the flame zone. The analysis of char materials can provide an insight into fire resistant performance. The morphologies of the char residues for film after MCC testing are examined by SEM. As shown in Fig. 5, the residual char for EA2 is flatter and more compact compared to EA1. Consequently, it is possible that OZrP and flame retardant have synergistic effect and could promote the formation of effective charring layer. The compact char structure is very important to general fire resistant properties of the films, which can prevent the heat transfer between the flame zone and the underlying substrate, and protect the substrate from heat.

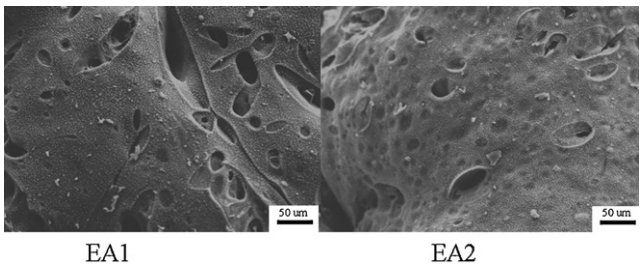

Fig. 5. SEM micrographs of the charred crusts: (a) EA1 and (b) EA2.

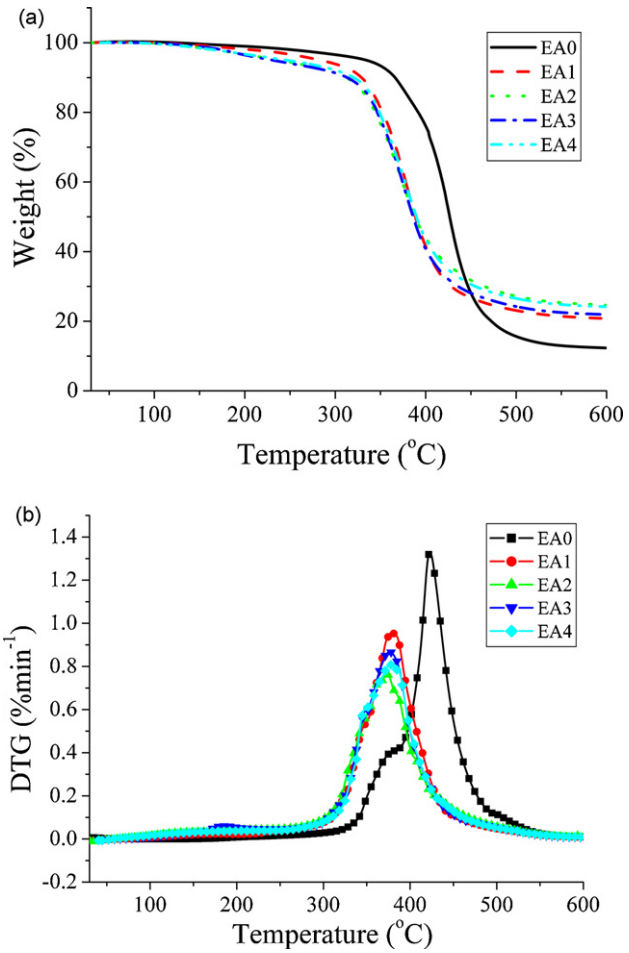

Fig. 6. TGA (a) and DTG (b) curves of the cured films under N_2.

4.4. Thermal behavior

TGA is one of the most widely used techniques for rapid evaluation of the thermal stability for various polymers [34,35]. Fig. 6 gives the thermogravimetric analysis (TGA) and derivative TGA (DTG) curves for the flame retardant EA composites. The data for the temperature at which 10% ($T_{-10\%}$) thermal degradation occurs, and the temperature of the maximum mass loss rate (T_{max}) obtained from the DTG curves, are listed in Table 2. The TGA curves display an onestep degradation process for pure EA and EA/FR composites. It can be seen that the decomposition temperature at 10% weight loss ($T_{-10\%}$) of UV-cured flame retardant films are earlier than pure EA, suggesting that FR destabilizes EA at lower temperature. As shown in Fig. 6(b), the T_{max} for EA/FR samples also decreases compared with neat EA. This can be explained by a chemical reaction between EA and flame retardant, which could accelerate the degradation of EA to form the stable char at lower temperature, resulting in the decrease of peak of mass loss rate. Hence, after 450 °C, the flame retardant films are more thermally stable than the sample pure EA.

Table 2
The thermogravimetric analysis data of the cured films.

Sample	Temperature at specific weight loss (°C) $T_{-10\%}$	T_{max} (°C)	Residue (%) at 600 °C
EA0	366	422	12.3
EA1	328	381	20.8
EA2	311	373	24.6
EA3	313	376	21.9
EA4	320	378	24.2

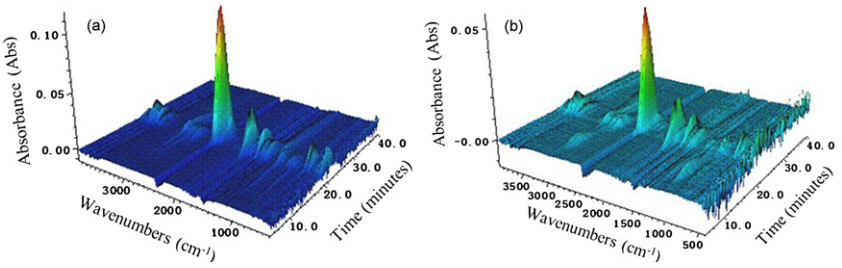

Fig. 7. The 3D surface graph for the FTIR spectra of the evolved gases produced by EA1 (a) and EA2 (b) pyrolysis.

The char yield of the pure EA is 12.3% at 600 °C, whereas the amount of the solid residue for EA1 film is 20.8%.

The partial replacement of FR by OZrP at the same total loading of 40% for FR + OZrP, results in the deterioration of the thermal stability in terms of $T_{-10\%}$. The probable reasons may be that the intimate contacts between the polymer molecules and the atoms of the inorganic crystalline layers in EA2, EA3 or EA4 are more extensive. And at the same time, there is a catalytic role played by the layered phosphate deriving from the Hoffman degradation of C_{16}, which may accelerate the charring process at the beginning of the degradation [36]. But there is an increase for nanocomposites in char formation at 600 °C, and EA2 has the most char residue (24.6%) among resins. This means that OZrP could promote residual char to further form the carbonaceous material. On the other hand, the OZrP platelets disperse very well in the polymer matrix and hinder the movement of polymer chains. Meanwhile, the introduction of OZrP is efficient in lowering the peak of mass loss rate, as shown in Fig. 6(b), especially EA2. It can be ascribed that EA2 generates the fewer evolved products and releases the little heat at T_{max}. The result is in good agreement with the above-mentioned MCC study.

4.5. The evolved products of the UV-cured films

The TGA-IR technique that directly gives identification of the evolved products can significantly contribute to an understanding of thermal degradation mechanism [37]. The evolved products formed during the thermal degradation of EA1 and EA2 films were characterized by TGA-IR.

Fig. 7 shows 3D TGA-IR spectra of gas phase in thermal degradation of EA1 (a) and EA2 (b) at heating rate 20 °C min^{-1} in nitrogen atmosphere. In Fig. 7, peaks in the regions of around 3400–4000 cm^{-1}, around 2700–3000 cm^{-1}, around 2250–2350 cm^{-1}, around 1600–1900 cm^{-1}, around 1250–1500 cm^{-1}, and around 1000–1100 cm^{-1} are noted. The spectra fit well to the reported FTIR features of gas products such as H_2O (3400–4000 cm^{-1}), hydrocarbons (2800–3000 cm^{-1}), CO_2 (2300 cm^{-1}), CO (2140 cm^{-1}), and carbonyl (1741 cm^{-1}, 1446 cm^{-1}).

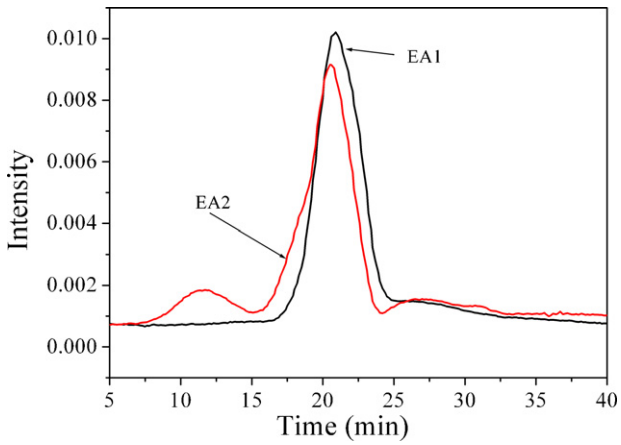

Fig. 8. The total evolved products versus time for EA1 and EA2.

The change for the intensity of the total evolved products versus time is shown in Fig. 8. It can be seen that the intensity for EA/FR/OZrP (EA2) is lower than that of EA/FR (EA1). It could be ascribed that the evolved products of EA2 are less than EA1, i.e., EA2 is more stable. It implies that the process of thermal degradation for EA2 is influenced by OZrP, and there may be a synergistic effect between FR and OZrP. It is very interesting that there are two peaks in EA2 curve. The first peak is ascribed to the degradation of OZrP. The second is assigned to the degradation of film itself.

In order to further study the difference between EA1 and EA2, some IR evolution curves of the identified gaseous species are shown in Fig. 9. H_2O and CO_2 are easily identified by their characteristic absorbance: H_2O at around 3540 cm^{-1}; CO_2 at around 2300 cm^{-1}. The data obtained from EA1 and EA2 can be compared quantitatively as the weight of sample during the testing of each sample is kept constant (1 mg). As shown in Fig. 9, the intensities of

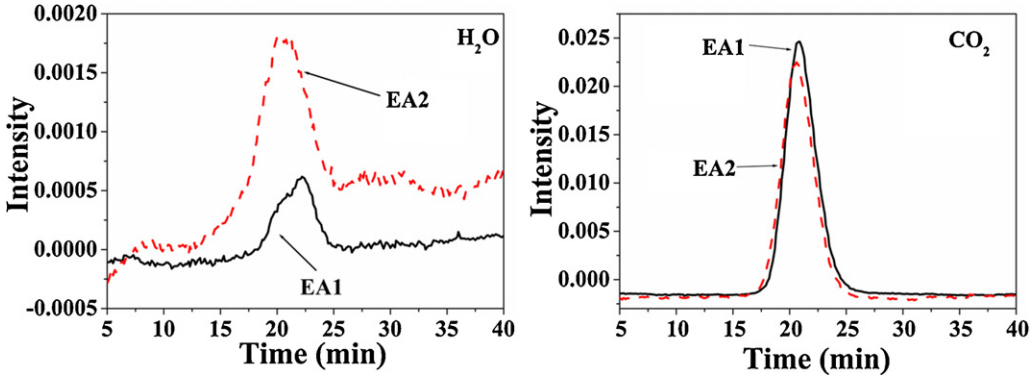

Fig. 9. Relationship between intensity of characteristic peak and time for evolved CO_2 and H_2O.

CO_2 for EA1 are higher than that of EA2. It is further said that OZrP could hinder the decomposition of flame retardant films. It is very interesting that the evolved water for EA2 is more than EA1, which could dilute and cool the flammable volatiles. This could further enhance the flame retardancy of EA2 and reduce the heat release rate. Hence, the thermal stability for EA2 is enhanced due to the addition of OZrP at the higher temperature.

5. Conclusions

In conclusion, the flame retardancy and thermal stability of UV-curable epoxy acrylate nanocomposites based on organophilic α-ZrP were studied. Their microstructures were investigated by XRD and TEM. Results showed that OZrP were well dispersed in the EA matrix. In the MCC tests, the nanocomposites showed a significant reduction in the heat release capacity (HRC) and peak heat release rate (PHRR) compared with both pure EA and the flame-retarded film without OZrP. During thermal degradation, EA1 was easily decomposed and released more gaseous compounds compared with EA2. The presence of OZrP could retard the movement and scission of the main chain of matrix resin during thermal degradation process. SEM showed that OZrP might promote to form the stable and smooth char layer in the condensed phase, which could prevent the underlying materials from further degradation.

Acknowledgements

The work was supported by the Program for Specialized Research Fund for the Doctoral Program of Higher Education (200803580008), the Program for Science and Technology of Suzhou (SG-0841), the Opening Project of State Key Laboratory of Environmental Adaptability for Industrial Product, and the Program for the graduate innovation fund in University of Science and Technology of China.

References

[1] T.Y. Ìnan, E. Ekinci, A. Kuyulu, A. Güngör, Polym. Bull. 47 (2002) 437.
[2] M.V. Kahraman, G. Bayramoğlu, N. Kayaman-Apohan, A. Güngör, React. Funct. Polym. 67 (2007) 97.
[3] T.H. Chiang, T.E. Hsieh, React. Funct. Polym. 68 (2008) 601.
[4] R.W. Truss, P.J. Hine, R.A. Duckett, Composites A 28 (1997) 627.
[5] S.A. Page, R. Mezzenga, L. Boogh, J.C. Berg, J.E. Månson, J. Colloid Interf. Sci. 222 (2000) 55.
[6] Th. Randoux, J.Cl. Vanovervelt, H. Van den Bergen, G. Camino, Prog. Org. Coat. 45 (2002) 281.
[7] H.S. Park, D.W. Kim, K.H. Hwang, B.S. Yoon, J.P. Wu, J.W. Park, H.S. Hahm, W.B. Im, J. Appl. Polym. Sci. 80 (2001) 2316.
[8] T.H. Ho, H.J. Hwang, J.Y. Shieh, M.C. Chung, React. Funct. Polym. 69 (2009) 176.
[9] D. Price, K. Pyrah, T.R. Hull, G.J. Milnes, J.R. Ebdon, B.J. Hunt, P. Joseph, Polym. Degrad. Stab. 77 (2002) 227.
[10] D. Price, K. Pyrah, T.R. Hull, G.J. Milnes, W.D. Wooley, J.R. Ebdon, B.J. Hunt, C.S. Konkel, Polym. Int. 49 (2000) 1164.
[11] H.B. Liang, A. Asif, W.F. Shi, J. Appl. Polym. Sci. 99 (2006) 3130.
[12] S.W. Zhu, W.F. Shi, Polym. Degrad. Stab. 81 (2003) 233.
[13] H.B. Liang, A. Asif, W.F. Shi, Polym. Degrad. Stab. 87 (2005) 495.
[14] S.C. Lv, W. Zhou, H. Miao, W.F. Shi, Prog. Org. Coat. 65 (2009) 450.
[15] J. Ma, Z.Z. Yu, Q.X. Zhang, X.L. Xie, Y.W. Mai, I. Luck, Chem. Mater. 16 (2004) 757.
[16] A.H. Gemeay, I.A. Mansour, R.G. El-Sharkawy, A.B. Zaki, Eur. Polym. J. 41 (2005) 2575.
[17] D.Y. Tang, L.S. Qiang, Z. Jin, W.M. Cai, J. Appl. Polym. Sci. 84 (2001) 709.
[18] L.Y. Sun, W.J. Boo, D.Z. Sun, A. Clearfield, H.J. Sue, Chem. Mater. 19 (2007) 1749.
[19] K. Zahouily, C. Decker, S. Benfarhi, J. Baron, Proc. RadTech. North. Am. (2002) 309.
[20] F. Bauer, R. Flyunt, K. Czihal, H. Ernst, S. Naumov, M.R. Buchmeiser, Nucl. Instrum. Meth. B 265 (2007) 87.
[21] A. Clearfield, G.D. Smith, Inorg. Chem. 8 (1969) 431.
[22] J. Alongi, A. Frache, Polym. Degrad. Stab. 95 (2010) 1928.
[23] L.S. Brandao, L.C. Mendes, M.E. Medeiros, L. Sirelli, M.L. Dias, J. Appl. Polym. Sci. 102 (2006) 3868.
[24] W.J. Boo, L.Y. Sun, J. Liu, A. Clearfield, H.J. Sue, J. Phys. Chem. C 111 (2007) 10377.
[25] R. Zhang, Y. Hu, L. Song, Y.R. Zhu, W.C. Fan, Z.Y. Chen, Chin. J. Nonferr. Metals 11 (2001) 895.
[26] H.B. Liang, W.F. Shi, Polym. Degrad. Stab. 84 (2004) 525.
[27] Y. Tang, W.W. Shan, G.M. Zeng, M. Peng, Thermosetting Resin 20 (2005) 13.
[28] US Patent 6,464,391.
[29] Standard Test Method for Heat and Visible Smoke Release Rates for Materials and Products, ASTM E 906, American Society for Testing and Materials, West Conshohocken, PA, 1998.
[30] P.M. Hergenrother, C.M. Thompson, J.G. Smith Jr., J.W. Connell, J.A. Hinkley, R.E. Lyon, R. Moulton, Polymer 46 (2005) 5012.
[31] H. Zhang, P.R. Westmoreland, R.J. Farris, E.B. Coughlin, A. Plichta, Z.K. Brzozowski, Polymer 43 (2002) 5463.
[32] W.Y. Xing, L. Song, P. Lv, G.X. Jie, X. Wang, X.Q. Lv, Y. Hu, Mater. Chem. Phys. 123 (2010) 481.
[33] M. Le Bras, S. Bourbigot, Fire Mater. 20 (1996) 191.
[34] K. Fukushima, M. Murariu, G. Camino, P. Dubois, Polym. Degrad. Stab. 95 (2010) 1063.
[35] A. Fina, D. Tabuani, G. Camino, Eur. Polym. J. 46 (2010) 14.
[36] M. Zanetti, T. Kashiwagi, L. Falqui, U. Camino, Chem. Mater. 14 (2002) 881.
[37] F. Bellucci, G. Camino, A. Frache, A. Sarra, Polym. Degrad. Stab. 92 (2007) 425.